Navier-Stokes Prediction of the Effect of the Skids on the Aerodynamics of Helicopter Fuselage in Forward Flight

W. Khier

Institute of Aerodynamics and Flow Technology
German Aerospace Center (DLR)
Lilientahlplatz 7, 38108 Braunschweig, Germany

email: walid.khier@dlr.de

Abstract

A series of three-dimensional Navier-Stokes computations were carried out with and without skids to investigate the influence of the skids on the flow field and aerodynamic forces acting on a helicopter fuselage in low Mach number forward flight under different pitch angles. All the numerical results presented in the paper were produced using multi-block structured grids and a finite volume approach. The computed aerodynamic forces were significantly improved with respect to their experimental counterparts by the inclusion of the skids in the computational model.

1. Introduction

Due to functional requirements, most helicopters in service nowadays have an aerodynamically inefficient, bluff fuselage design, which usually results in large separation regions, and aerodynamic interaction between the different components of the aircraft. Enhancing the design of a helicopter requires a detailed understanding of its aerodynamic characteristics.

There are two established approaches available nowadays to provide such understanding: wind tunnel testing and computational fluid dynamics (CFD). Wind tunnel measurements have been relied upon for decades to predict, analyse and improve the performance of future helicopters. It provides a clear impression on the aerodynamic forces acting on the object being investigated. However, wind tunnel experiments are highly complex and cost demanding. In addition, interpretation of experimental data is not a straight forward process, and involves extensive empirical corrections. Measurement of surface data and visualisation of the flow field contribute significantly to the complexity, and thus, to the overall costs of the measurements. CFD offers an attractive remedy to the above shortcomings. Therefore, it has been gaining ground in the rotorcraft research and development environment over the past few decades. Early research efforts concentrated on the individual elements of the aircraft [1-5]. Although still computationally expensive for routine use nowadays, Khier *et al.* [6] and Visingardi *et al* [7,8] demonstrated the capability of CFD to study the interaction between the moving components in helicopter and tilt rotor configurations.

However, despite the reported advances, CFD cannot be used to analyse any class of flow problems without a thorough validation by experimental results. Previous

validations of CFD results [13] revealed consistent deviation from the experimental counterparts for the whole range of pitch angles considered. One possible reason for the deviation was the exclusion of the skids in the simulation. Therefore, in the present paper a numerical investigation of the effects of the skids on the resulting flow field and aerodynamic forces is presented based on the solution of the Reynolds averaged Navier-Stokes equations in three dimensions. The computations correspond to wind tunnel measurements of an Eurocopter BO-105 fuselage (Figure 1) under Mach number of 0.135 forward flight conditions at various pitch angles.
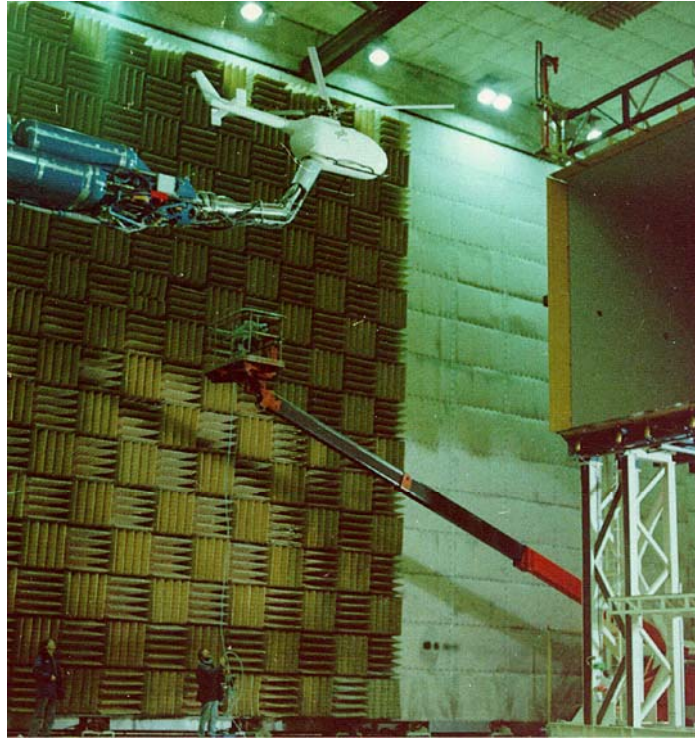

Figure 1: BO105 1:2.5[th] scale wind tunnel model

2. The numerical approach

The Reynolds (Favre)-Averaged Navier-Stokes equations are solved by means of the CFD simulation code FLOWer developed at DLR since the beginning of the 90's. The solution process is based on Jameson's method where a second order central scheme is used for the discretisation of the convective fluxes. A stabilizing blend of second and fourth order dissipation is added to the fluxes of the main flow equations [10-12], and a first order accurate Roe's scheme is employed to compute the convective fluxes of the turbulence equations. Steady state solution is obtained iteratively by integrating the equation in a fictitious time using multi-stage Runge-Kutta method. The solution process makes use of acceleration techniques like local time stepping, multigrid and implicit residual smoothing.

Turbulence effects may be introduced either by Second Moment Closure (SMC), also known as Reynolds Stress Models (RSM), or by using Boussinesq's Eddy Viscosity approach (EVM). Among the various eddy viscosity and RSM models available, two equation models are a reasonable compromise between accuracy and computational costs. For aeronautic applications the two-equation k-ω approach of Wilcox [9]

proved superior to k-ε eddy viscosity model class, which utilizes the dissipation rate ε as the scale-determining quantities rather than the specific turbulence dissipation rate, ω.

However, two-equation models are known of their excessive production of eddy viscosity owing to the Boussinesq's assumption, which leads to positive production of the turbulence kinetic energy regardless of the state of strain. As a result, excessive turbulent mixing may stabilizes boundary layers against adverse pressure gradients, delaying or completely preventing flow separation. Similarly, unsteadiness of the flow may also be suppressed for the same reason. In the present study both the Wilcox and Menter's SST [10] variants of k-ω model are used to emphasize the effect of turbulence modelling on the computed results.

No-slip and farfield (one-dimensional characteristic theory) boundary conditions for the mean flow equations are set respectively on solid bodies, and on remote surfaces. No assumptions are made for the boundary layer profile, rather, the equations of motion are integrated down to the wall (*Low-R*e approach). On solid surfaces, the turbulence kinetic energy k is set equal to zero, and the specific dissipation rate, ω, is obtained from the equilibrium between dissipation and diffusion of ω in the viscous sub-layer.

3. Geometrical Characteristics and Grid Generation

Analogous to the actual wind tunnel model, all surface details of the real helicopter were excluded from the computations. Only those components of the fuselage with major aerodynamic function were retained, namely, the spoiler, skids and horizontal stabilizer. The model support was included in the simulation to account for the flow blockage on the lower side properly.

The construction of a structured multiblock mesh around complex geometries is a tedious task. Overlapping grid (Chimera) technique reduces the effort required for mesh generation considerably by decomposing complex configurations into a number of simpler elements. In this study, the computational configuration was subdivided into four groups: the fuselage, left stabilizer, right stabilizer, and strut and spoiler. Conventional multi-block structured grids were generated around each group individually by trilinear interpolation. Elliptic smoothing was applied subsequently to improve the quality of the initial grid. In order to facilitate grid generation further, all child grids are embedded in an automatically generated, locally adapted Cartesian background grid. Communication among the different grid components is realized by applying Chimera: First, all points lying within grid overlap regions are excluded from the solution procedure, leading to the creation of new boundaries inside each component grid. Flow data are exchanged between the different components on these special boundaries by interpolation. A search operation is performed to identify the most suitable donor points for each point on the Chimera boundaries. A detailed overview of the procedure is given in detail in [13] and [14]. Figure 2 shows the intersection of the component grids with the Cartesian background grid at symmetry plane.

The component grids consist of 48 blocks (Fuselage: 17, Strut+Spoiler: 9, left and right stabilizers: 5 each, left and right skids 12 in total) and a total number of 6.58 Million point. The background grid consisted of 297 blocks and 1.72 Million points.
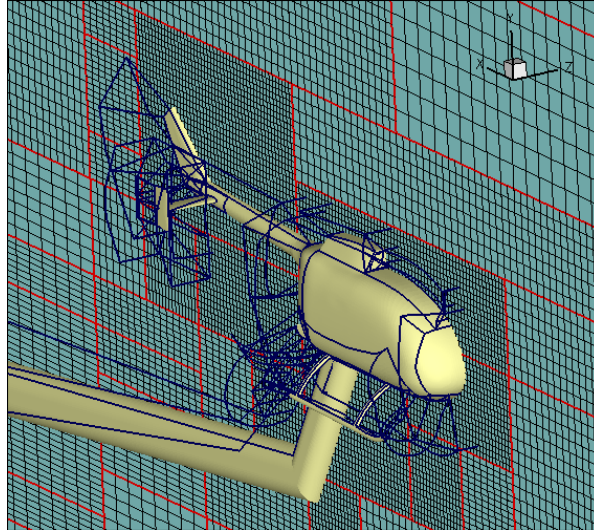
Figure 2: Multi-Block structured Chimera component grids around the fuselage

4. Results and Discussion

The wind tunnel tests used a 40% Mach-scaled model based on the EuroCopter BO-105 Helicopter. The measurements included both isolated fuselage and fuselage-rotor configurations under a wide variety of flight conditions. Hover as well as forward flight tests were performed for speeds up to 46.5 m/sec, and a tip Mach number equal to 0.641. Four test facilities were used to assess the effect of the blocking ratio and other tunnel related factors under different pitch angles. The test procedure and results are reported in [15] and [16]. A full description of the test stand and its main components is given in [17-18].

Four test cases were selected from the experimental campaign for this study. All four cases correspond to forward flight at the same flow conditions except the angle of attack, which was successively reduced from nose up flight at 8.17^o for case TC1 to -6.94^o for case TC4 at a step of approximately 5 ^{o}. A summary of the test cases is contained in Table 1.

Test Case	α	Re (Million)	Ma_∞
TC1	8.17^o	8.51	0.136
TC2	3.14^o	8.51	0.136
TC3	-1.87^o	8.51	0.136
TC4	-6.94^o	8.51	0.136

Table 1: Experimental test matrix. α is the pitch angle in degrees. Reynolds number is based on a model length of 3.5 m

Pressure coefficient distribution at symmetry plane is shown in Figure 3 for the four test cases with and without skids. The figure compares computed results obtained by Wilcox and SST models with the experimental values.

On the upper surface, the two turbulence models behave similarly in the nose region regardless of the pitch angle and the presence of the skids. There is a slight

improvement in pressure produced by SST in the wind shield and roof area. Wilcox model overestimates the pressure rise in front of the engine fairing in TC1 and TC2. This trend is reversed in TC4. It is not quite clear which model behaves better on the leading upper edge of the engine fairing as there is no sufficient experimental data to evaluate the suction peaks predicted by the two models. The lowest pressure is predicted by Wilcox model equal to -4.65 in TC3. The pitch angle does not seem to play a major role on the suction peak except for very low pitch values as in TC4. SST model recovers the pressure faster on the engine fairing showing slightly better agreement with measurements in TC1. The differences become less significant as the pitch angle is reduced. Downstream of the engine fairing no considerable differences between the models can be observed, and both models show fairly good agreement with the experiment for all pitch angles. The skids do not seem to influence the pressure significantly on the upper side except in TC2 where higher pressures are predicted by both models at the root of the tail fin.

On the lower surface the flow accelerates over the nose causing a reduction in pressure up to X =-0.27, followed by a gradual deceleration then a steep increase in pressure due to the strut. The computed pressure lags the experiment in this region. It was not clear at the time of performing the computations that a slip ring assembly was mounted in front of the strut in the experiment. The presence of the slip rings introduced additional blockage effect below the fuselage, which was not reproduced by the computations. Apart from this geometrical inconsistency, both models show comparable accuracy upstream of the strut. Noticeable differences can be seen only in the immediate vicinity of the strut, where a slightly higher pressure is predicted by Wilcox's model. No experimental data is available for the region downstream of the strut and up to one third of the tail boom. Within this region, the performance of Wilcox's model is influenced by the skids, whereas SST model yielded negligible changes in pressure when the skids were added. A similar situation as on the upper surface is observed along the tail boom. Both models show almost equal deviation from experiment.

Figure 4 illustrates the computed and measure surface pressure at a cross section 0.066 m upstream of the skids (X = -0.277). The figure shows a significant effect of the skids on the upper surface pressure predicted by SST, which is a bit surprising. The difference between SST results with and without skids starts small at TC1 (α =8.17°) and increases with a reduction of α reaching a maximum of 0.2 in TC4 (α =-6.94°). Wilcox"s model results in a better agreement with the experimental data in comparison to SST, and does not seem to be sensitive to the presence of the skids.

On the lower side two pressure peaks can be observed at Z = ±0.25 indicating the stagnation effect introduced in the flow by the skids. The increase in C_p has a magnitude of about 0.25 and varies slightly with the pitch angle. Both models predict a pressure pattern similar to that found in the experiment. In the central region Wilcox's model is generally in better agreement with the experiment than SST model, which underestimate the pressure showing a difference of 0.05 to 0.09 in C_p (except for case TC3). As for the peak pressure both models predict the peak values with a comparable accuracy. However, the location of the peaks is shifted towards the symmetry plane by Wilcox's model as the pitch angle decreases.
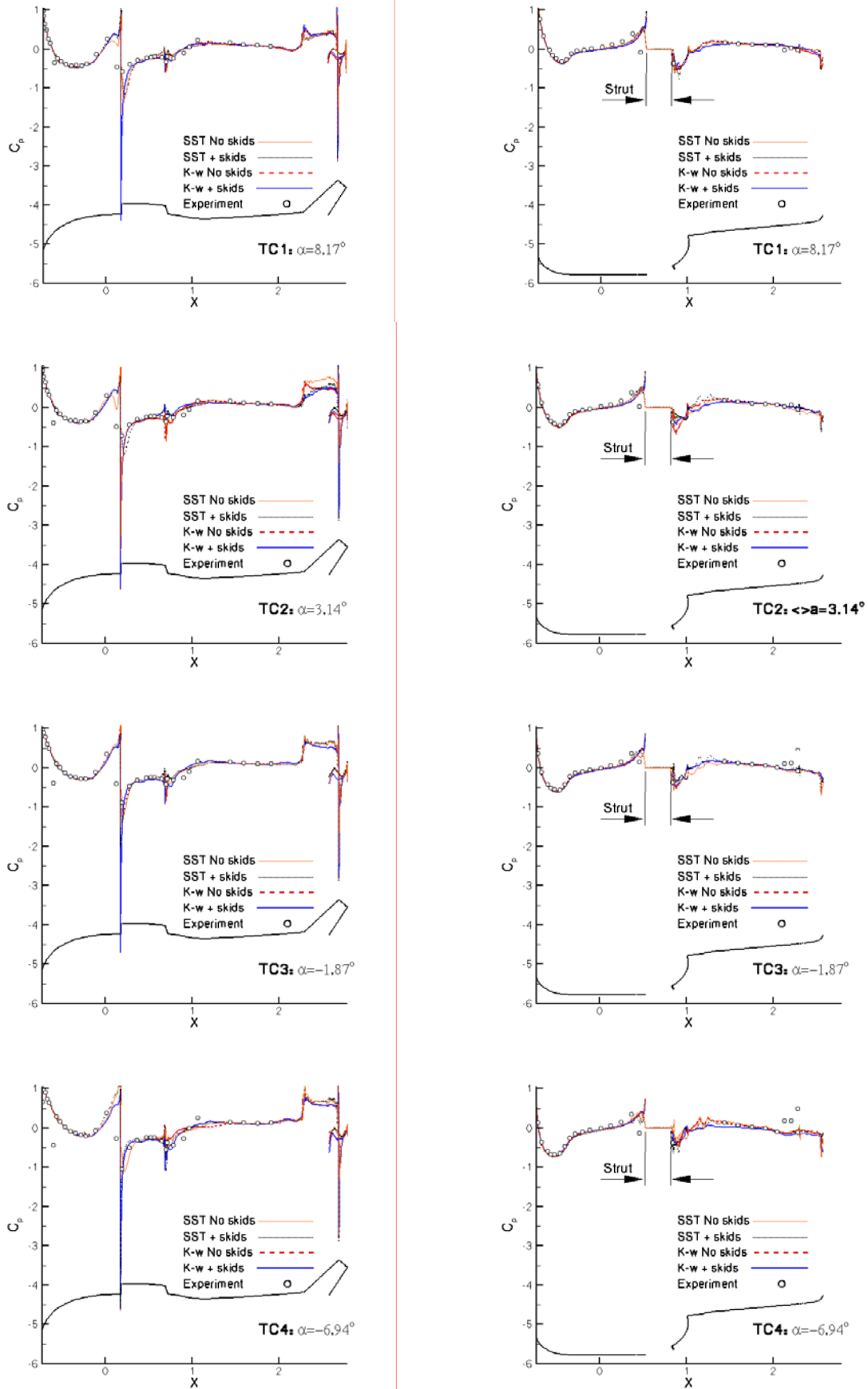
Figure 3: Pressure coefficient distribution at symmetry plane as a function of the pitch angle. Left: Upper side. Right: Lower side
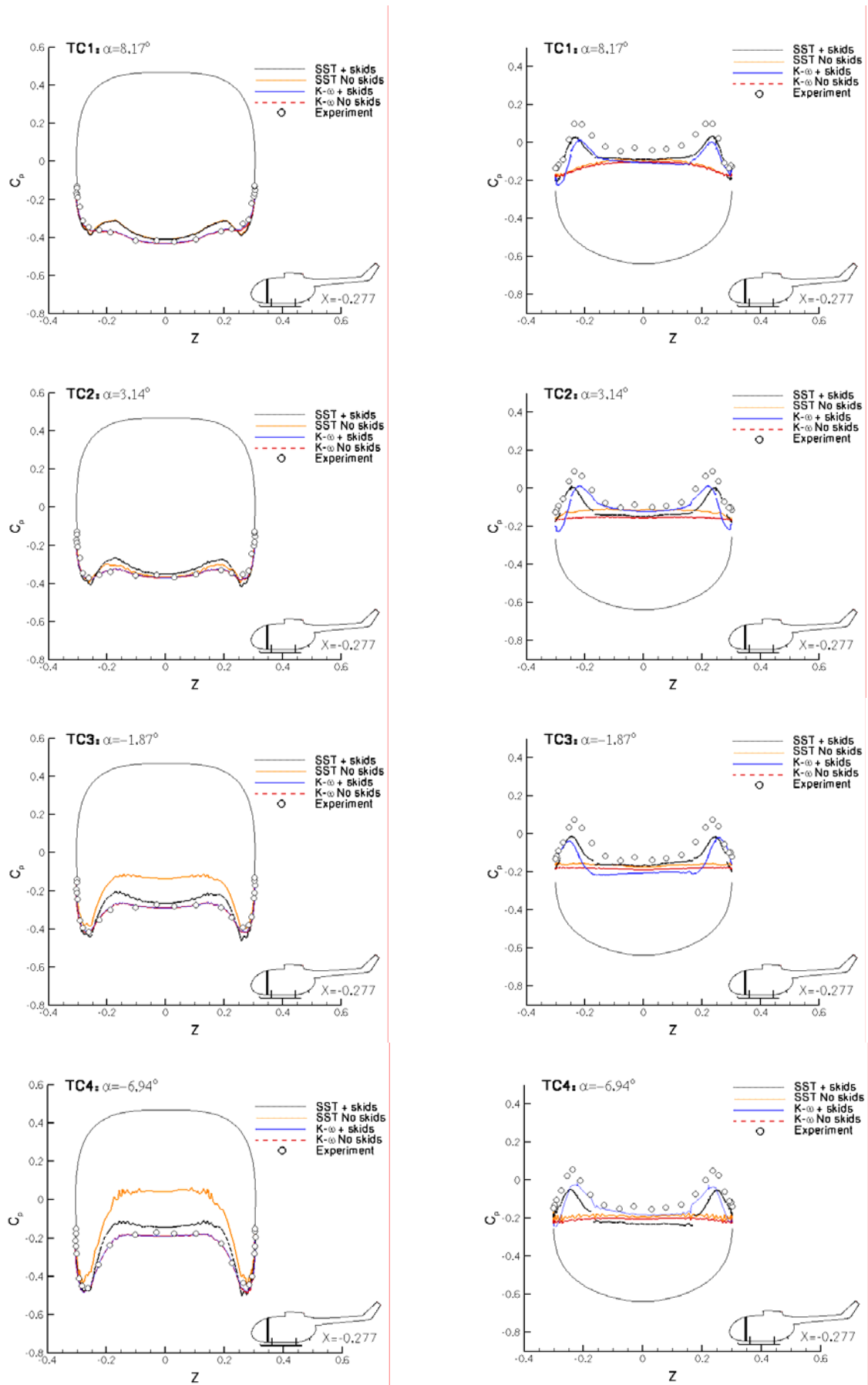
Figure 4: Comparison between computed and measured surface pressure at constant X = -0.277. Left: Upper side, Right: Lower side

A totally different trend results in the absence of the skids where an almost constant pressure is predicted by both models. A slight increase in pressure is observed in the central area in TC1 probably due to the large pitch angle.
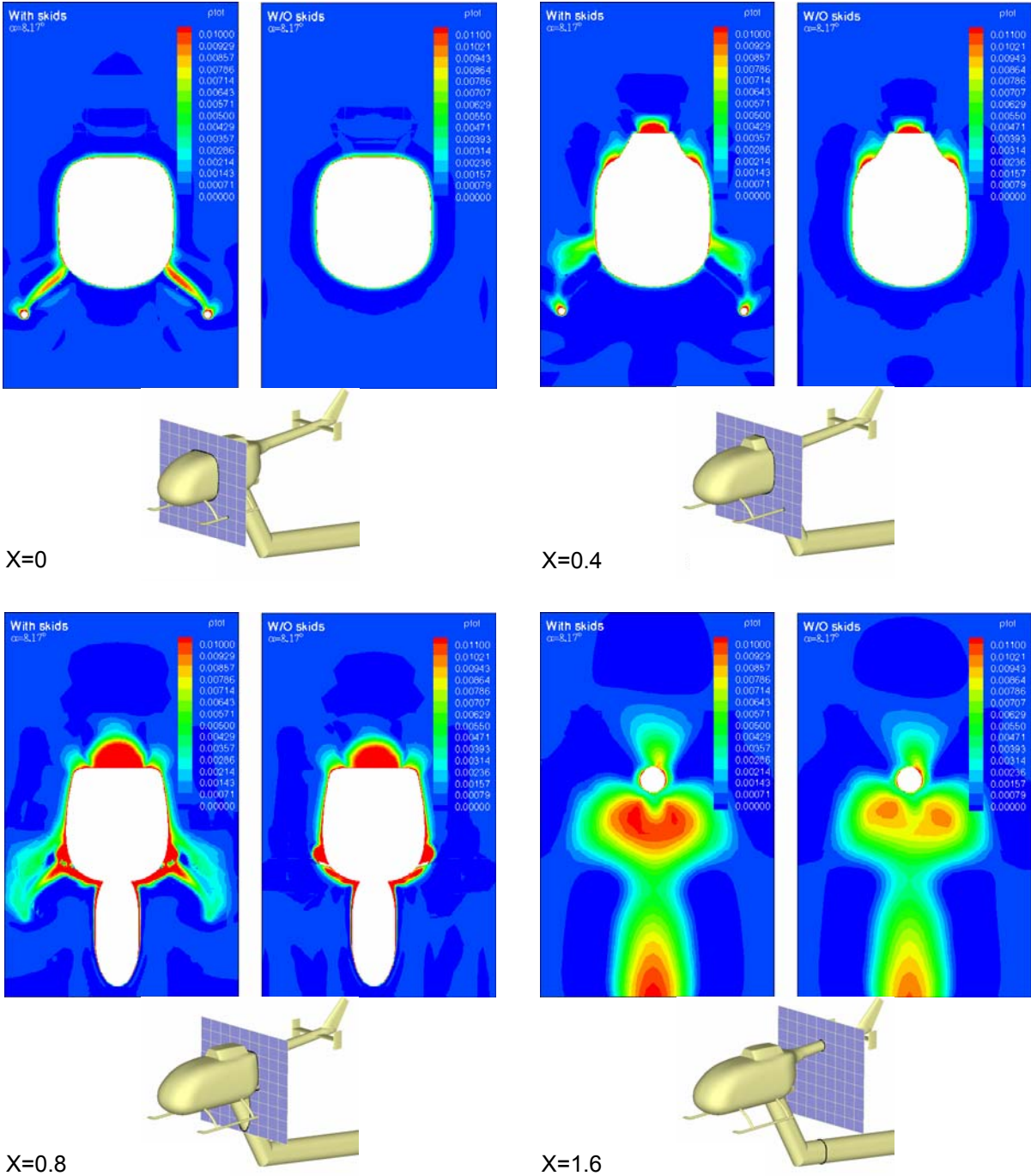

X=0

X=0.4

X=0.8

X=1.6

Figure 5: Total pressure loss in the fuselage wake at selected cross sections for TC1 ($\alpha=8.17^{o}$)

In addition to the previously mentioned flow blocking effect, the skids alter the wake structure significantly as can be deduced from total pressure loss contours shown by Figure 5. The figure illustrates the total pressure loss computed by SST model for TC1 at selected cross sections, X = 0, 0.4, 0.8 and 1.6. From the figure the evolution of the wake of the skids can be seen. There is a narrow separation zone behind the front vertical supports of the skids at X=0 which moves up with the distance

downstream. At X=0.8 the wake structure becomes significantly complex. In addition to the vortex observed at X=0 and X=0.4, traces of vortices created by the rear vertical supports of the skids is observed, and interacts with the wake of the spoiler and the secondary corner vortices of the fuselage. On the upper side a higher total pressure loss is observed at X=0.8 in comparison to the case without skids. At X=1.6 no traces of the wake of the skids can be identified. However, high total pressure losses can be still observed.
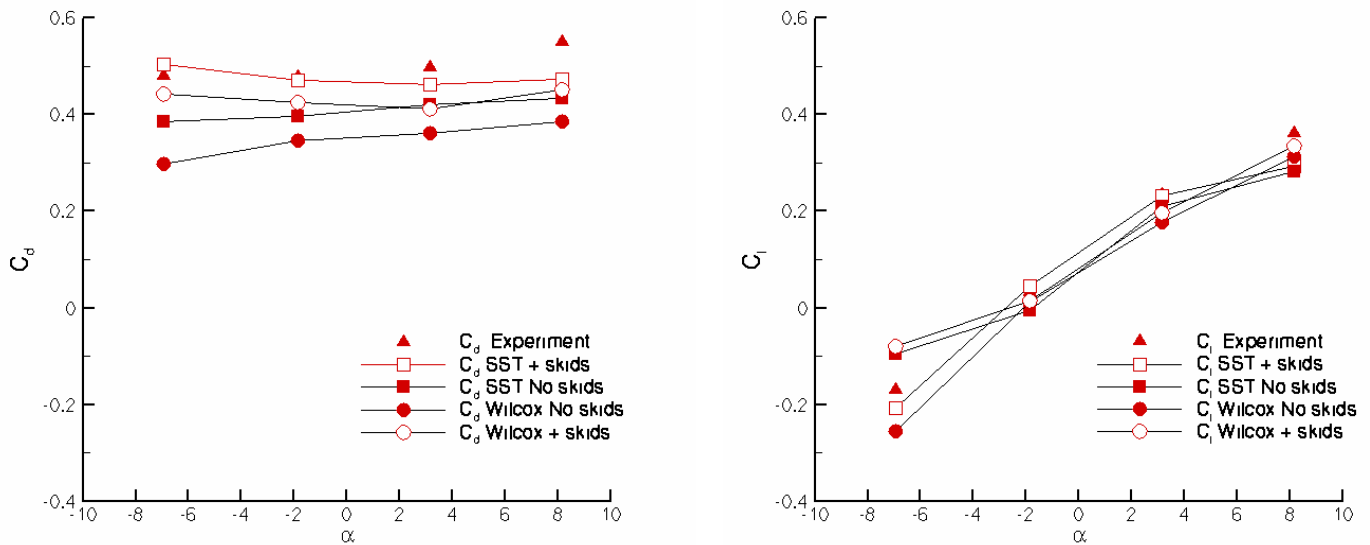

Figure 6: Variation of drag (left) and lift (right) with pitch angle.

	-6.94°	-1.87°	3.14°	8.17°
Experiment	0.479	0.478	0.496	0.548
Wilcox + Skids	0.442	0.423	0.411	0.450
SST + Skids	0.503	0.469	0.461	0.473
Wilcox No Skids	0.296	0.345	0.360	0.385
SST No Skids	0.385	0.395	0.421	0.432

Table 2: Summary of computed and measured drag coefficients

	-6.94°	-1.87°	3.14°	8.17°
Experiment	-0.170	0.031	0.234	0.361
Wilcox + Skids	-0.080	0.015	0.196	0.335
SST + Skids	-0.206	0.044	0.230	0.293
Wilcox No Skids	-0.255	0.011	0.177	0.313
SST No Skids	-0.096	-0.006	0.209	0.282

Table 3: Summary of computed and measured lift coefficients

The computed aerodynamic lift and drag coefficients are compared with their experimental counterparts in Figure 6 and listed in tables 2 and 3. Significant improvement in drag can be observed for the full configuration (with skids) using SST model. However, although SST model is quantitatively in a better agreement with the experiment, Wilcox's model predicts the experimental trend better showing continuous increase in drag with the pitch angle. For both models an increase in drag

is produced by the skids for the entire pitch angle range. Both models predict similar contributions of the skids to the drag coefficient except the very low pitch angle (α=-6.94 ^{o}) where SST predicts an increase of 0.146 in C_d while Wilcox's model predict 0.118.

Very good agreement with the experiment is found for the lift is computed by the SST model. The best agreement is observed for α=3.14^o with an error in C_l of only 1.7%. For α=8.17^o Wilcox's model predicts higher contribution of the skids to aerodynamic lift than SST. The agreement with experiment is also better for Wilcox's model at this angle where a deviation of 7% from the experiment was found, while SST predicts a C_l 13% less than the experimental value. At α=-6.94 ^{o} the two models behave in an opposite sense. While SST predicts a decrease in lift as a result of the skids, Wilcox's model produces higher lift when the skids are included in the simulation.

5. Summary and Conclusions

The effect of the skids on the flow and aerodynamic coefficients was studied and reported in this paper. Wicox's k-ω and SST models were applied to investigate the influence of turbulence modelling on the results under forward flight conditions at different pitch angles.

Detailed analysis of the results was carried out, which included pressure distribution and aerodynamic force comparisons with the experiment. In addition, a brief analysis of the computed total pressure losses in the wake was performed.

The investigation revealed negligible effect of the skids on the pressure distribution in the symmetry plane regardless of the turbulence model used. However, significant improvement in the agreement with experiment was achieved for cross sectional pressure on the lower side. For the cross section considered significant differences in computed pressure were produced by the skids in SST case on the upper side of the fuselage. A similar trend was not produced by Wilcos's model.

An analysis of the wake in terms of total pressure losses was carried out. Large areas of total pressure loss were generated behind the vertical supports of the skids and were transported downstream resulting in a complex wake pattern and intensive interaction with the fuselage and spoiler wakes.

The inclusion of the skids improved the agreement between measured and computed forces considerably. Aerodynamic coefficients obtained by SST were broadly in a better agreement with the experiment than those produced by Wilcox's model. However, Wilcox's model predicted the qualitative trend of the experimental drag more accurately than SST model. The best agreement in drag was achieved by SST for TC3 (α=-1.87 ^{o}) showing an error of only -1.8%. The most accurate lift coefficient was obtained in TC2 (α=3.14^o) also by SST with and error of -1.7%.

6. References

1. P. Beaumier, E. Chelli, K. Pahlke, Navier-Stokes Prediction of Helicopter Rotor Performance in Hover Including Aero-Elastic Effects, American Helicopter Society 56th Annual Forum, Virginia Beach, Virginia, May 2-4, 2000.

2. E. Chelli, K. Pahlke, Calculation of Viscous Flow Around the BO105 Main Rotor in Hover, DLR Internal Report IB-NR 129-99/27.

3. K. Pahlke, B. van der Wall, Calculation of Multibladed Rotors in High-Speed Forward Flight with Weak Fluid-Structure-Interaction, 27th European Rotorcraft Forum, 11-14 September 2001, Moscow, Russia.

4. H. Pomin, S. Wagner, Navier-Stokes Analysis of Helicopter Rotor Aerodynamics in Hover and Forward Flight, AIAA Paper 2001-0998.

5. H. Pomin, S. Wagner, Aeroelastic Analysis of Helicopter Rotor Blades on Deformable Chimera Grids, AIAA Paper 2002-0951.

6. W. Khier, T. Schwarz, J. Raddatz Time Accurate Simlation Of The Flow Around The Complete BO105 Wind Tunnel Model, 31th European Rotor Craft Forum, 13-15th Sept. 2005, Florence, Italy.

7. A. Visingardi, J. Decours, W. Khier, S. Voutsinas, Code-to-Code Comparison for the Blind Test Activity of the TILTAERO Project, 31th European Rotor Craft Forum, 13-15th Sept. 2005, Florence, Italy.

8. A. Visingardi, W. Khier, J. DecoursThe Blind Test Activity of TILTAERO Project for the Numerical Aerodynamic Investigation of a Tilirotor. European Congress on Computational Methods in Applied Sciences and Engineering, 24-28th July 2004, Jyväskylä, Finland.

9. D.C. Wilcox, Reassessment of the Scale-Determining Equation for Advanced Turbulence Models, AIAA Journal, vol. 26, no. 11;

10. F. R. Menter, Two-Equation Eddy Viscosity Turbulence Models for Engineering Applications}, AIAA Journal, 32(8) (1994) 1598 - 1605.

11. R. Radespiel, N. Kroll, Accurate Flux Vector Splittings for Shocks and Shear Layers, Journal of Computational Physics, 121, pp. 66-78, 1995.

12. R. Heinrich, K. Pahlke, H. Bleecke, A Three-Dimensional Dual-Time Stepping Method for the Solution of the Unsteady Navier-Stokes Equations, Proceedings of the Conference on Unsteady Aerodynamics, July 17-18th, 1996, London, UK.

13. W. Khier, T. Schwarz, Application of Cartesian Background Grid in combination with Chimera Method to predict Aerodynamics of Helicopter Fuselage. 29th European Rotor Craft Forum, 16-18th Sept. 2003, Friedrichshafen, Germany.

14. T. Schwarz, Berechnung der Umströmung einer Hubschrauber-Rumpf-

Konfiguration auf der Basis der Euler-Gleichungen mit der Chimären-Technik, DLR Internal Report IB-NR 129-97/23.

15. H. J. Langer, R. L. Peterson, T. H. Maier, An Experimental Evaluation of Wind Tunnel Wall Correction Methods for Helicopter Performance, American Helicopter Society 52nd Annual Forum, Washington, D.C., June 4-6, 1996.

16. B. Junker, H. J. Langer: Private communication.

17. V. Mikulla, Improved Experimental and Theoretical Tools for Helicopter Aeromechanic and Aeroacustic Interactions (HELIFLOW)}, Report No.: HFLOW/3/ECD/01, 1997.

18. W. R. Splettstoesser, B. Junker, K.-J. Schultz, W. Wagner, W. Weitemeyer, A. Protopsaltis, D. Fertis. The HELINOISE Aeroacoustic Rotor Test in the DNW - Test Documentation and Representative Results, DLR-Mitteilung 93-09.